Photoacoustics 30 (2023) 100457

Contents lists available at ScienceDirect

Photoacoustics

journal homepage: www.elsevier.com/locate/pacs

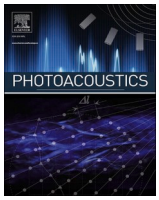

Multispectral optoacoustic tomography of the human intestine – temporal precision and the influence of postprandial gastrointestinal blood flow

Lars-Philip Paulus [a,b], Alexandra L. Wagner [a,b], Adrian Buehler [a,b], Roman Raming [a,b], Jörg Jüngert [a], David Simon [c], Koray Tascilar [c], Alexander Schnell [a], Josefine Günther [d], Ulrich Rother [d], Werner Lang [d], André Hoerning [a], Georg Schett [c], Markus F. Neurath [e], Joachim Woelfle [a], Maximilian J. Waldner [e], Ferdinand Knieling [a,b], Adrian P. Regensburger [a,b,*]

[a] Department of Pediatrics and Adolescent Medicine, University Hospital Erlangen, Friedrich-Alexander-Universität (FAU) Erlangen-Nürnberg, Erlangen, Germany
[b] Pediatric Experimental and Translational Imaging Laboratory (PETI-Lab), Department of Pediatrics and Adolescent Medicine, University Hospital Erlangen, Friedrich-Alexander-Universität (FAU) Erlangen-Nürnberg, Erlangen, Germany
[c] Department of Medicine 3 and German Center Immunotherapy (DZI), University Hospital Erlangen, Friedrich-Alexander-Universität (FAU) Erlangen-Nürnberg, Erlangen, Germany
[d] Department of Vascular Surgery, University Hospital Erlangen, Friedrich-Alexander Universität (FAU) Erlangen-Nürnberg, Erlangen, Germany
[e] Department of Medicine 1 and German Center Immunotherapy (DZI), University Hospital Erlangen, Friedrich-Alexander-Universität (FAU) Erlangen-Nürnberg, Erlangen, Germany

ARTICLE INFO

Keywords:
Optoacoustic
Photoacoustic
Multispectral optoacoustic imaging
Inflammatory bowel disease
Gut
Reliability
Reproducibility
Intestinal blood flow
Postprandial

ABSTRACT

Multispectral optoacoustic tomography (MSOT) holds great promise as a non-invasive diagnostic tool for inflammatory bowel diseases. Yet, reliability and the impact of physiological processes during fasting and after food intake on optoacoustic signals have not been studied. In the present investigator initiated trial (NCT05160077) the intestines of ten healthy subjects were examined by MSOT at eight timepoints on two days, one fasting and one after food intake. While within-timepoint and within-day reproducibility were good for single wavelength 800 nm and total hemoglobin (ICC 0.722–0.956), between-day reproducibility was inferior (ICC −0.137 to 0.438). However, temporal variability was smaller than variation between individuals (coefficients of variation 8.9%−33.7% vs. 17.0%−48.5%). After food intake and consecutive increased intestinal circulation, indicated by reduced resistance index of simultaneous Doppler ultrasound, optoacoustic signals did not alter significantly. In summary, this study demonstrates high reliability and temporal stability of MSOT for imaging the human intestine during fasting and after food intake.

1. Introduction

Non-invasive imaging of human organs for diagnosis, disease assessment and treatment response monitoring is an integral component of modern medicine. Emerging label-free, non-ionizing, bed-side imaging modalities like optoacoustic imaging (OAI) are very well suited for these purposes. OAI uses pulsed laser light to induce thermoelastic expansion in molecules, which produces pressure waves that can be recorded, visualized and quantified [1]. By using light at multiple wavelengths and spectral unmixing algorithms, multispectral optoacoustic tomography (MSOT) can distinguish different chromophores, such as oxygenated and deoxygenated haemoglobin [2].

Various preclinical and clinical studies have already demonstrated the potential of OAI for assessing inflammatory diseases in children and adults [3–5]. In patients with inflammatory bowel diseases (IBD), increased hemoglobin signals correlated well with disease severity [6,7], as vasodilatation and increased blood flow is a hallmark of acute inflammatory processes [8,9].

Especially in transabdominal OAI, the influence of physiological changes and potential confounders on optoacoustic signals have not been investigated, yet. This information could improve the interpretation of optoacoustic signal alterations in the inflamed intestine.

Previously, OAI data obtained from muscle imaging showed good intra- and interrater reliability and reproducibility over time [10,11].

* Correspondence to: Pediatric Experimental and Translational Imaging Laboratory (PETI-Lab), Department of Pediatrics and Adolescent Medicine, University Hospital Erlangen, Friedrich-Alexander-Universität (FAU) Erlangen-Nürnberg, Loschgestr. 15, 91054 Erlangen, Germany.
E-mail address: adrian.regensburger@uk-erlangen.de (A.P. Regensburger).

https://doi.org/10.1016/j.pacs.2023.100457
Received 30 September 2022; Received in revised form 29 January 2023; Accepted 1 February 2023
Available online 2 February 2023

Notably, muscle activation showed a transient influence on the acquired signals [10]. Similar changes might also be expected in the intestine after food intake and at different phases of digestion. As known from previous studies, postprandial gastrointestinal blood flow increases locally with the transit of food through the digestive tract, from 10 to 30 min after food intake in the stomach, 120 min in the ileum, and 200–300 min in the colon [12–15].

In this prospective study we investigated the reproducibility of MSOT for imaging the human intestine over time and physiological changes – caused by fasting or food intake – of the optoacoustic signals within the bowel wall.

2. Materials and methods

2.1. Study design and participants

In this prospective single-center investigator initiated trial, ten healthy volunteers have been repeatedly examined by MSOT and Doppler ultrasound during fasting and after food intake. The study was approved by the local ethics committee (346_21B), registered (clinicaltrials.gov ID NCT05160077), and performed in accordance with the Declaration of Helsinki. Each subject gave written informed consent prior to participation.

Healthy individuals at or above 18 years of age were eligible for this study. Subjects were recruited from the local periphery by public announcement. Subjects were excluded in case of pregnancy, nursing, tattoos at imaging sites, subcutaneous fat tissue thickness over 3 cm, acute or chronic diseases of the gastrointestinal tract or symptoms suggestive of such a disease, or diseases requiring acute treatment.

After collection of demographic data (such as sex and age), each subject went through three consecutive study arms (I: fasting, II: standardized meals, and III: standardized meals with Indocyanine green) on three different days with at least 48 h in between. Study arm III will be published separately as experimental pilot study accompanied by extensive phantom experiments. In this analysis, we present the first two study arms (study arm I performed on day A and study arm II performed on day B) (Fig. 1). Study arm I and II comprised the following examination protocol: All examinations started at 8:00 / 8:30 am after a fasting period of at least ten hours. Imaging was performed at eight timepoints (t0 to t7) with an interval of 60 min in between.

2.2. Study procedures

At each timepoint the examination protocol included the measurement of pulse rate and arterial blood pressure, MSOT imaging of the gastric antrum, terminal ileum, transverse colon, sigmoid colon, and Doppler sonography of the splanchnic arteries (celiac artery and superior mesenteric artery). The inferior mesenteric artery was not assessed because repeated anatomic localization would have been too inconsistent and time-consuming in this study protocol due to its anatomical localization, accompanied by gas and stool overlay.

Before MSOT imaging of the gastric antrum, 150 ml of water was ingested to achieve a homogenous filling of the stomach on every imaging timepoint to facilitate transabdominal imaging of the gastric wall. Every anatomical position was scanned twice by MSOT (v1 and v2). On study day A, subjects remained in fasting state throughout all eight imaging timepoints. Study day B included two standardized meals, similar to continental breakfasts to mimic physiologic eating habits (for women 500 kcal and for men 650 kcal, containing 55% carbohydrates, 29% fat and 16% proteins, supplementary Table 1**)** [16], after the first and fifth imaging timepoint (Fig. 1).

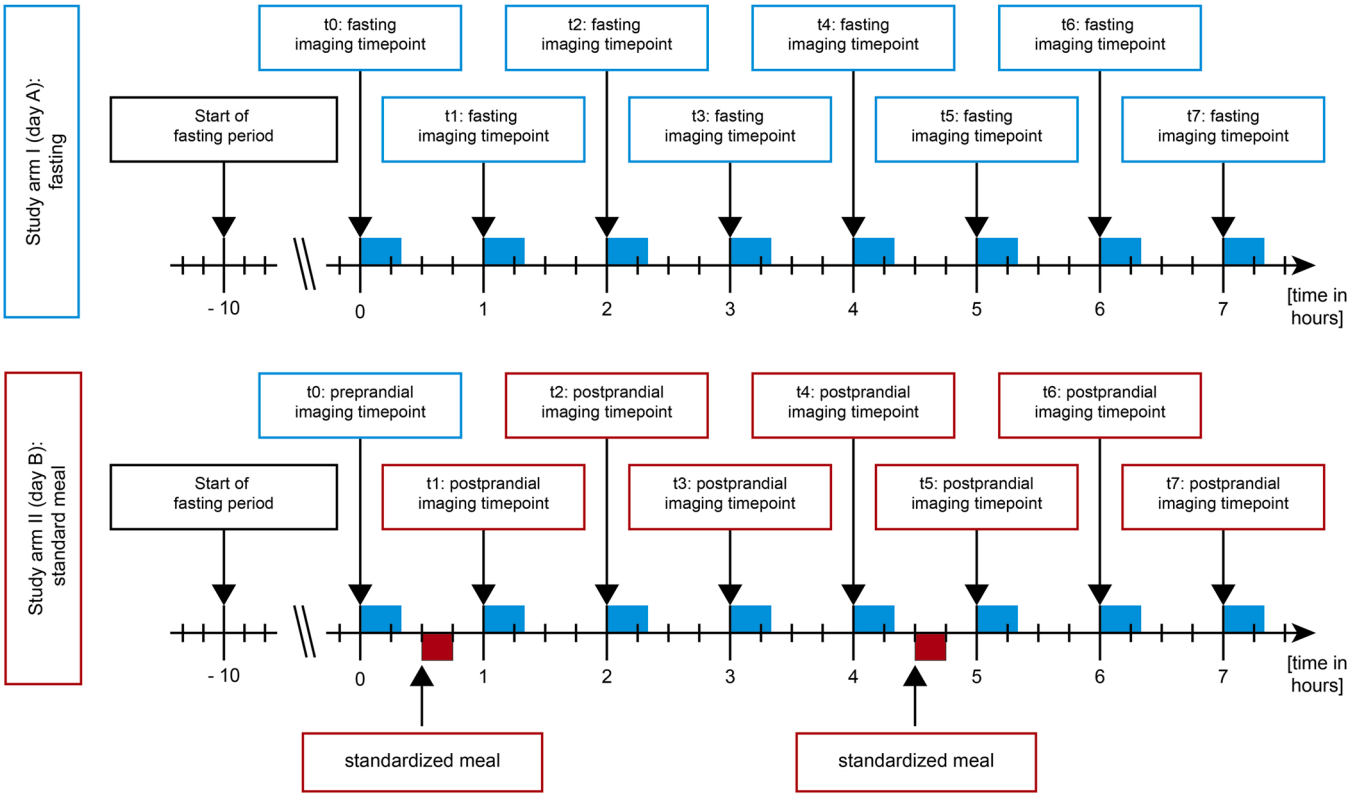

Fig. 1. Study flow. Ten healthy subjects were assigned to both study arms I (day A) and II (day B). After ten hours of fasting each subject underwent eight imaging timepoints (t0 – t7) with intervals of 60 min on day A (fasting) and day B (with standardized meals 30 min after the first and fifth imaging timepoint). Each examination lasted about 20 min.

2.3. MSOT Device

MSOT imaging was performed by a single CE-certified MSOT Acuity ECHO system (iThera medical GmbH, Munich, Germany). The system contains a handheld 2D detector with a class 4 laser with output wavelengths from 660 to 1300 nm and a pulse repetition rate of 25 Hz. The field of view was 4 × 4 cm, with a penetration depth up to 2.5 cm. In this study six single wavelengths (SWL; 700, 730, 760, 800, 850, and 900 nm) were recorded.

During optoacoustic imaging, the system simultaneously acquires interleaved ultrasound image frames by Reflection ultrasound computed tomography (RUCT), which is used for anatomical guidance during live imaging and region of interest (ROI) placement. The displayed optoacoustic signals during live imaging allow quality control during image acquisition. The signal quantification within the ROIs enables detection of optoacoustic signals derived from blood vessels in human intestine.

The detector was always positioned above the skin and coupled by transparent ultrasound gel (Aquasonic Clear, MDSS GmbH, Hannover, Germany). For safety reasons, laser safety goggles were used by all attending persons and any adverse events were recorded.

2.4. Data analysis

Directly after each imaging timepoint, ROIs were placed at the MSOT imaging system by the investigator. All polygonal ROIs were drawn around the superficial bowl wall (Fig. 2C). Thereafter, the data was transferred to the institutional data server and further processed with iLabs software V 1.3.6 (iThera medical GmbH, Munich, Germany). Prior to signal quantification, all ROIs were checked by two readers.

After the final ROI placement, all scans were processed using the same method with a batch processing software iLabs. MSOT signals in a. u. for SWL and unmixed MSOT parameters were quantified. For spectral unmixing, linear regression algorithm was used to unmix deoxygenated hemoglobin (HbR) and oxygenated hemoglobin (HbO2) [1]. Total hemoglobin (HbT) and oxygen saturation (mSO2) were quantified on a pixel-by-pixel basis as HbT = HbR + HbO2, and mSO2 = HbO2 / HbT. Additionally, pixels of the 0.5% lowest HbT were discarded from the mSO2 quantification to reduce obscurity from noise.

2.5. Ultrasound

For ultrasound imaging a Siemens Acuson X300 (Siemens Medical Solutions Inc., Mountain View, USA), equipped with a curved array transducer (CH5–2), and a GE Logiq E9 (GE Healthcare, Wauwatosa, USA), equipped with curved array transducer (C1–6), were used. All subjects were investigated as follows: first, the abdominal aorta with the origins of the celiac artery and superior mesenteric artery (SMA) was visualized. Then, the diameter and pulsed-wave-Doppler measurements (peak systolic velocity, end diastolic velocity, and resistance index) of both arteries were obtained.

2.6. Statistics

Descriptive data were summarized as counts, percentages or mean ± standard deviation (SD) as appropriate. Sample size was not calculated due to the pilot character of the study. Coefficients of variation (CVs) were calculated as the ratio of SD to the mean.

Intraclass correlation coefficients (ICCs) with two-way mixed effects, absolute agreement, single measurement model was used for calculation of within-timepoint reliability. Within-day and between-day reliability was assessed by ICCs with two-way mixed effects, absolute agreement, multiple measurements model. The grading was according to Landis and Koch (<0.00 = poor, 0.00–0.20 = slight, 0.21–0.40 = fair, 0.41–0.60 = moderate, 0.61–0.80 = substantial, 0.81–1.00 = almost perfect) [17].

In advance to further calculations, normal distribution of data was tested by Shapiro Wilk test. As appropriate, one-way ANOVA or mixed effects analysis for data sets with missing data and Turkey's post hoc test or Friedman test and Dunńs multiple comparisons test were used. Depth correlation is presented as Pearson correlation coefficient (r). Gender differences were analyzed by unpaired T-test or Man-Whitney-U test, accordingly.

For all calculations a P value < 0.05 was used to indicated statistical significance. ICCs were calculated using IBM SPSS Statistics (Version 28.0.0.0, International Business Machines Corporation, Armonk, USA), all other statistical tests were performed with GraphPad Prism (Version 9, GraphPad Software Inc., La Jolla, USA).(Table 1).

3. Results

3.1. Demographic and clinical characteristics

Ten healthy subjects (n = 6 female) were enrolled between November 2021 and January 2022. The mean demographic and clinical characteristics of the study population is shown in Table 2. All subjects completed all MSOT and ultrasound imaging timepoints (Fig. 1). The MSOT principle is illustrated in Fig. 2A.

3.2. Reliability of MSOT imaging

In total, n = 1280 MSOT scans were acquired from four anatomical regions of ten healthy volunteers at eight imaging timepoints (t0 to t7) on two study days each (A and B, Fig. 1). On every imaging timepoint, two scans (v1 and v2) of the same region were recorded in direct sequence. Seven scans from day A were excluded, as anatomical identification was not possible or scans were missing. Optoacoustic SWL signals (700, 730, 760, 800, 850 and 900 nm) and MSOT parameters (HbR, HbO2, HbT and mSO2) were quantified within the region of interest (Figs. 2B and 2C). Exemplary MSOT and RUCT images of the intestine are presented in Fig. 2C.

3.2.1. MSOT within-timepoint reliability

Intraclass correlation coefficients (ICCs) of n = 635 pairs (v1 and v2) were computed to investigate within-timepoint reliability (5 pairs were excluded due to missing of v1 and/or v2). When considering each anatomical region individually, within-timepoint reliability of the gastric antrum and transverse colon was superior to the terminal ileum, while ICCs of the sigmoid colon were the highest. ICCs of all SWL and MSOT parameters of the sigmoid colon (ICC range 0.821–0.894), SWL 700–850 nm, HbR and HbT of the gastric antrum (ICC range 0.805–0.870) and SWL 700–800 nm of the transverse colon (ICC range 0.816–0.834), were almost perfect. All other ICCs including all SWL and MSOT parameters of the terminal ileum were substantial (ICC range 0.677 – 0.793) (Fig. 3A and supplementary Table 2 - 5). After this section all regions were investigated separately for SWL 800 nm, HbT – corresponding to the main chromophore in the target tissue – and ROI depth and means from v1 and v2 were used for further calculations. In the following sections each mean of v1 and v2 was considered as one datapoint.

3.2.2. MSOT within-day reliability

Within-day reliability was tested by calculating ICCs of eight consecutive imaging timepoints during fasting (day A). A total of 318 datapoints (ten subjects with four anatomical regions scanned at eight timepoints) were used for the calculations. ROI depths were consistent over time in all anatomical regions (ICC range 0.908–0.986). Temporal reproducibility within one day of SWL 800 nm and MSOT parameter HbT was almost perfect (ICC range 0.863–0.956). In detail, ICCs of the gastric antrum and transverse colon were higher compared to the terminal ileum and sigmoid colon (e.g., ICCs for SWL 800 nm 0.921 and 0.956 vs 0.889 and 0.914, respectively). Furthermore, ICCs of SWL 800 nm were higher compared to ICCs of HbT in the terminal ileum, transverse colon and sigmoid colon (e.g., ICCs of terminal ileum 0.889 vs

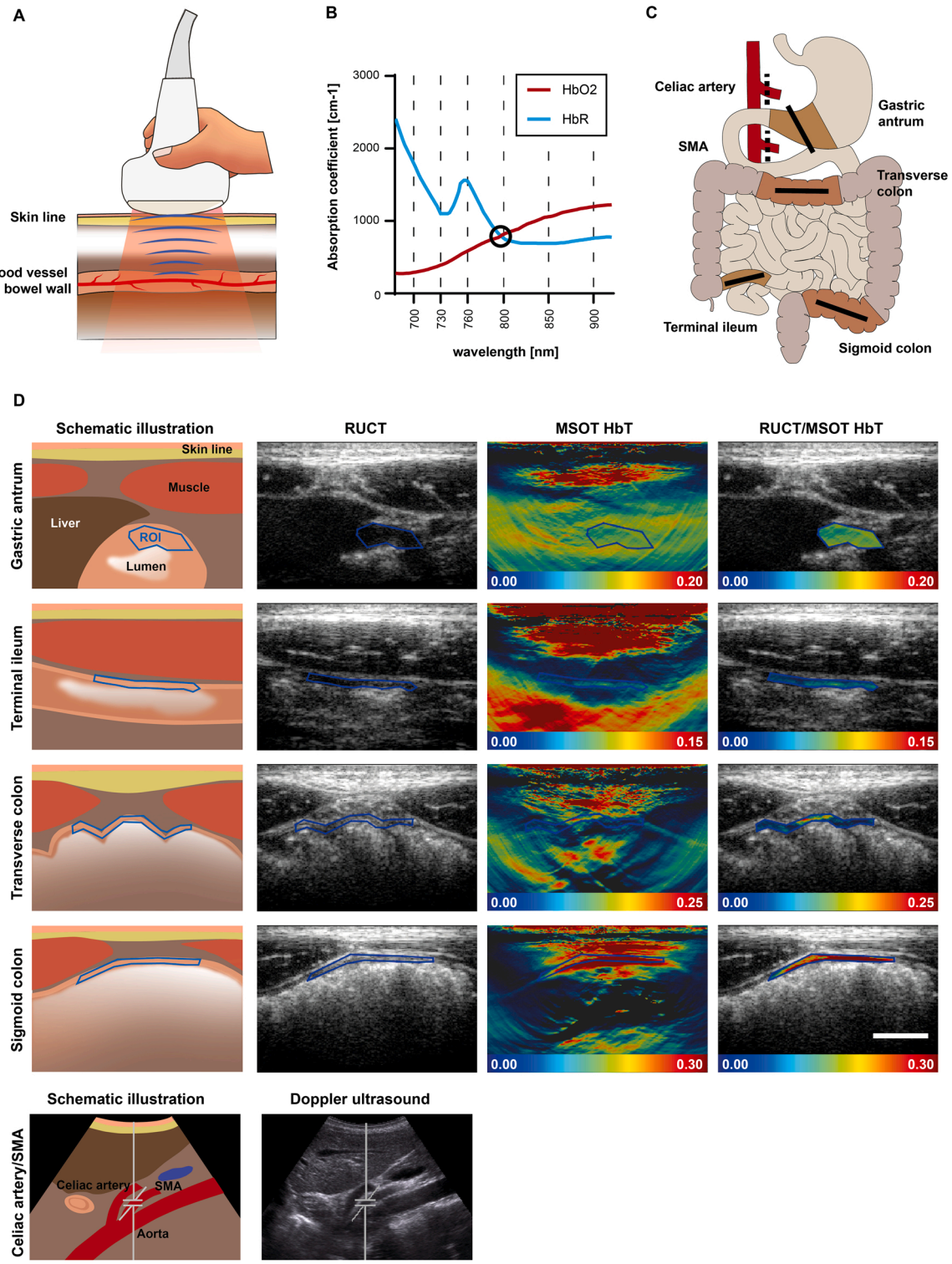

Fig. 2. MSOT imaging of the human intestine. A Illustration of MSOT imaging of the bowel wall. A handheld 2D detector illuminates the targeted tissue with pulsed laser light. After absorption and thermoelastic expansion ultrasound waves, particularly from hemoglobin molecules in blood vessels, can be detected and quantified. B Application of multiple wavelengths (700, 730, 760, 800, 850, and 900 nm) and spectral unmixing allows signal quantification of endogenous absorbers such as oxygenated (HbO2) and deoxygenated hemoglobin (HbR). At a wavelength of 800 nm both absorbers (HbO2 and HbR) have their isobestic point, marked with a black circle (data derived from https://omlc.org/spectra/hemoglobin/summary.html, accessed 18.07.2022). C Illustration of the investigated locations. On each imaging timepoint, each subject underwent MSOT / RUCT imaging of gastric antrum, terminal ileum, transverse colon, and sigmoid colon (solid lines) and Doppler ultrasound of the celiac artery and superior mesenteric artery (SMA, dotted lines). D Exemplary MSOT/RUCT and ultrasound images of the intestine are presented with a respective schematic illustration. Live RUCT images are used for anatomical guidance of the investigator. Signal quantification is derived from a region of interest (ROI) drawn in the RUCT image after scan acquisition. MSOT parameter total hemoglobin (HbT) is displayed within the ROI to better visualize the signal intensities in the bowel wall. Scale bar indicates 1 cm.

Table 1
Demographic and clinical characteristics of study population.

Sex, female (n, %)	6, 60%
Age (years)	22.5 ± 1.2
Height (cm)	174.7 ± 9.1
Weight (kg)	66.5 ± 7.8
BMI (kg/m^2)	21.7 ± 1.1
Blood pressure systolic / diastolic (mmHg)	130.0 ± 10.4 / 70.9 ± 7.4
Puls rate (beats per minute)	61.8 ± 8.4

Data are presented as numbers, percentage or mean ± standard deviation.

0.863) (Fig. 3B and supplementary Table 6).

Additionally, coefficients of variation (CVs) across all timepoints were calculated for each subject and then averaged across all subjects. These between-timepoint CVs display the spread of measurements over time. Considering all locations together, the smallest variation was seen in ROI depth (CV 11,5%), followed by SWL 800 nm (18.4%) and HbT (25.2%). When calculated for each anatomical region individually, the gastric antrum and transverse colon showed lower CVs compared to the terminal ileum and sigmoid colon (e.g., CVs of 800 nm 14.9% and 13.4% vs 26.8% and 18.7%, Table 2).

3.2.3. MSOT between-day reliability

Between-day reproducibility was described using the ICCs of the first imaging timepoint of day A and B (80 datapoints, ten subjects with four anatomical regions at two timepoints). Herein, SWL 800 nm and HbT of the gastric antrum (ICC 0.430 and 0.438) and the terminal ileum (ICC 0.410 and 0.430) showed a moderate agreement. However, agreement for SWL 800 nm and HbT was fair for the sigmoid colon (ICC 0.388 and 0.287) and slight/poor for the transverse colon (ICC 0.167, 0.137). Agreement of ROI depth was very good for the gastric antrum, good for the transverse colon and moderate for the terminal ileum and sigmoid colon (ICC 0.937, 0.781, 0.553 and 0.445, Fig. 3C and supplementary Table 7). The scattered wide range of optoacoustic signals, despite good anatomical relocation, is exemplified for the transverse colon in Fig. 3D. However, between-day variations of optoacoustic signals were in the same range compared to between-timepoint variation on day A (CVs 15.2–26.9% vs 13.4–33.7% Table 2).

3.2.4. Between-subject variation

To compare the variation of MSOT measurements over time with the physiological variation between subjects, between-subject CVs were calculated for every timepoint of day A and averaged across all timepoints. These between-subject CVs for SWL 800 nm and HbT generally ranged higher (21.9–48.5%) compared to between-timepoint (13.4–33.7%) and between-day CVs (15.2–26.9%) for all anatomical regions (Table 2).

3.3. Influence of food intake and intestinal postprandial blood flow on MSOT signals

To elucidate the influence of food intake on optoacoustic signals of the human intestine, all subjects consumed two standardized meals (one after t0 and one after t4). A statistically significant difference was found in the gastric antrum between fasting and the two measurements after the second meal for SWL 800 nm (t0 vs t5 154.0 a.u. vs 160.6 a.u., $P = 0.0146$, and t0 vs. t6 154.0 a.u. vs. 174.0 a.u., $P = 0.0051$) but not for HbT (Fig. 4A). In contrast, all other anatomical regions did not show statistically significant signal alterations after food intake (all $P > 0.05$, Fig. 4A). Corresponding analyses of day A did not show any signal differences, too (all $P > 0.05$, Supplementary Fig. 1). In addition, variability of MSOT signals measured by between-timepoint CVs were in the same range on day A and day B (Table 2).

3.4. Influence of food intake and postprandial intestinal blood flow on Doppler sonography

Doppler ultrasound parameters were analyzed from 320 scans (ten subjects, two arteries, eight timepoints on two days) to evaluate alterations in gastrointestinal blood flow by changes of the resistance index (RI) in the celiac artery and superior mesenteric artery (SMA). The scans of two subjects ($n = 2 * 32$) and additional eleven scans were excluded due to obscurations of the splanchnic arteries by bowel gas, unfeasible anatomical identification, missing angle correction or missing scan.

During fasting, no significant changes of the resistance index in the celiac artery and SMA were found (all $P > 0.05$, Supplementary Fig. 1). After food intake, the resistance index of the celiac artery did not show statistically significant changes either. However, the resistance index of the SMA showed a statistically significant decrease after food intake (e.g., t0 vs t1, 0.87 vs 0.74, $P = 0.0027$) with subsequent rebound (e.g., t1 vs t3, 0.74 vs 0.84, $P = 0.0294$, Fig. 4B and supplementary Table 8). Meanwhile circulatory parameters (heart rate and blood pressure) stayed consistent (all $P > 0.05$, data not shown).

Detailed ultrasound measurements for all imaging timepoints are presented in the supplementary Table 9 and 10.

3.5. Depth correlation and gender differences

To analyze imaging depth as a potential confounder, a correlation between HbT and ROI depth was performed. For each subject the mean

Table 2
Coefficients of variation between timepoints and subjects.

	between-timepoint CV day A				between-timepoint CV day B			
	n	ROI depth	800 nm	HbT	n	ROI depth	800 nm	HbT
Gastric antrum	78	9.8%	14.9%	21.9%	80	10.2%	11.0%	14.4%
Terminal ileum	80	14.6%	26.8%	33.7%	80	15.6%	15.2%	21.3%
Transverse colon	80	7.5%	13.4%	20.2%	80	10.0%	8.9%	13.2%
Sigmoid colon	80	13.9%	18.7%	25.1%	80	16.8%	19.2%	27.8%
All locations	318	11.5%	18.4%	25.2%	318	13.2%	13.6%	19.2%
	between-day CV				**between-subject CV**			
	n	ROI depth	800 nm	HbT	n	ROI depth	800 nm	HbT
Gastric antrum	20	3.1%	15.2%	22.2%	78	17.0%	21.9%	33.0%
Terminal ileum	20	11.6%	21.5%	25.2%	80	20.4%	39.3%	48.5%
Transverse colon	20	9.3%	17.3%	26.4%	80	22.2%	22.9%	30.9%
Sigmoid colon	20	19.3%	19.4%	26.9%	80	28.0%	29.6%	34.9%
All locations	78	10.8%	18.3%	25.2%	318	21.9%	28.4%	36.8%

Coefficients of variation (CV) of region of interest (ROI) depth, single wavelength 800 nm and total hemoglobin (HbT) were calculated as the ratio of standard deviation to the mean. For between-timepoint CVs the CV of all timepoints of one day was calculated for each subject individually and then averaged across all subjects. Between-day CVs were computed accordingly with the first timepoints of day A and B. For between-subject CVs the CV of all subjects at each timepoint of day A was calculated and then averaged across all timepoints. Between-timepoint CVs represent the spread of data over time, while between-subject CVs describe the spread of data between individuals.

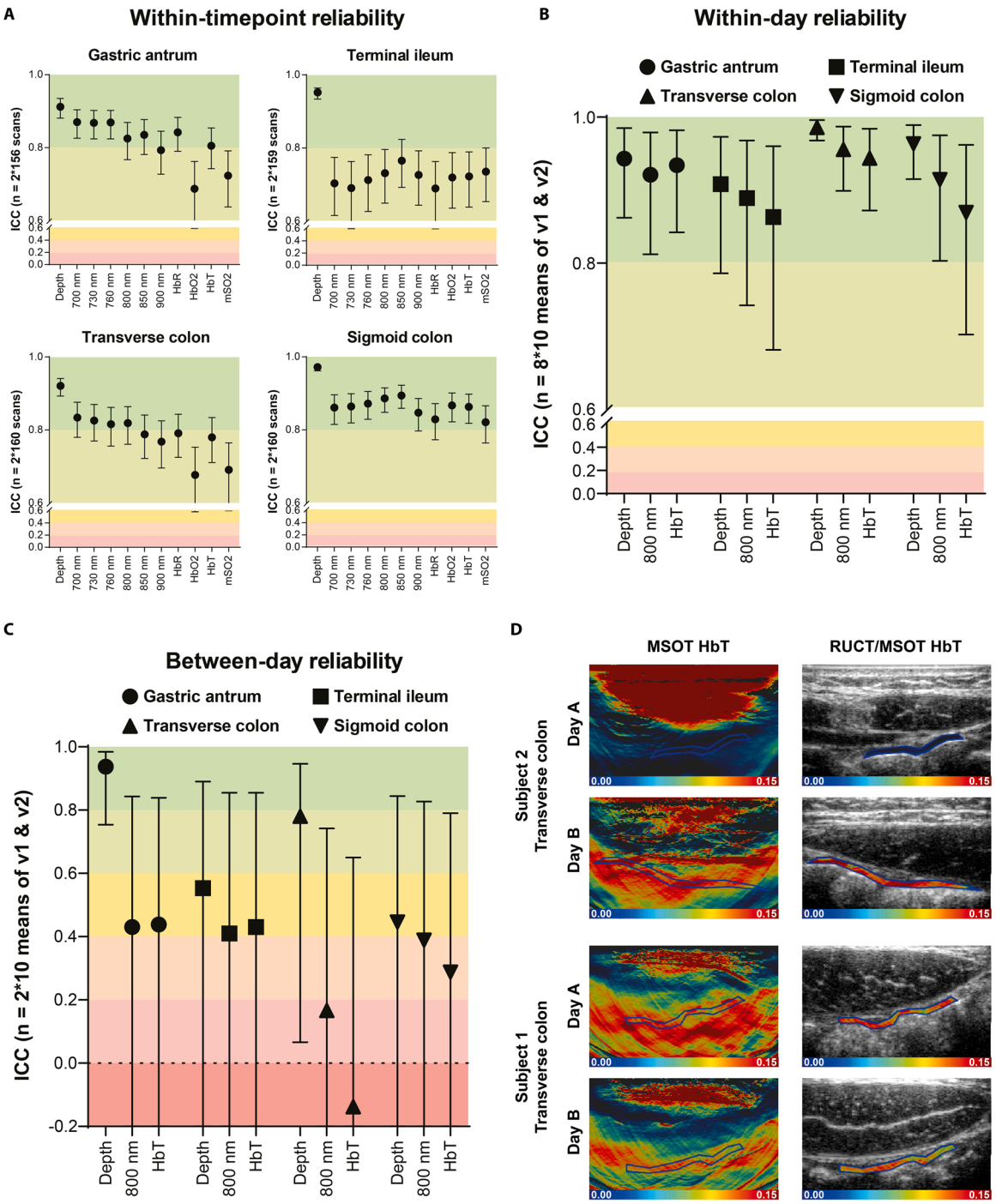

Fig. 3. Temporal reliability of MSOT signals in the human intestine A Within-timepoint reliability between two scans (v1 and v2) of the same timepoint. Intraclass correlation coefficients (ICCs) of region of interest (ROI) depth, single wavelengths (SWL) 700 nm, 730 nm, 760 nm, 800 nm, 850 nm, 900 nm and MSOT parameters deoxygenated hemoglobin (HbR), oxygenated hemoglobin (HbO2), total hemoglobin (HbT), and oxygenation saturation of hemoglobin (mSO2) are shown separated by anatomical region. Datapoints and whiskers represent ICCs and 95% confidence interval (CI) (Two-way mixed effects, absolute agreement, single measurement). ICCs were calculated from n = 2 * 160 scans for each anatomical region (two acquisitions, eight timepoints on two days each, ten subjects, seven scans excluded). B Within-day reliability between all timepoints (t0 – t7) on day A. ICCs of ROI depth, SWL 800 nm and HbT are shown separated by anatomical region. Datapoints and whiskers represent ICCs and 95% CIs (Two-way mixed effects, absolute agreement, average measures). ICCs were calculated from n = 8 * 10 data points for each anatomical region (eight timepoints, ten subjects, one datapoint derives from the mean of v1 and v2, two datapoints excluded). C) Between-day reliability between the first scan of day A and B. ICCs of ROI depth, SWL 800 nm and HbT are shown separated by anatomical region. Datapoints and whiskers represent ICCs and 95% CIs (Two-way mixed effects, absolute agreement, average measures). ICCs were calculated from n = 2 * 10 datapoints for each anatomical region (two timepoints, ten subjects, one datapoint derives from the mean of v1 and v2). A-C) ICC grading according to Landis and Koch: < 0.00 = poor, 0.00–0.20 = slight, 0.21–0.40 = fair, 0.41–0.60 = moderate, 0.61–0.80 = substantial, 0.81–1.00 = almost perfect. D) Exemplary MSOT/RUCT scans from the transverse colon on day A (t0) and day B (t0) are presented to demonstrate high anatomical relocation with different between-day agreement of MSOT signals. While one subject (1) showed deviating MSOT signal levels on day A and B (HbT day A vs. day B 0.0109 a.u. vs 0.1049 a.u.), a different subject (2) showed good agreement between both days (HbT day A vs. day B 0.1037 a.u. vs 0.1074 a.u.).

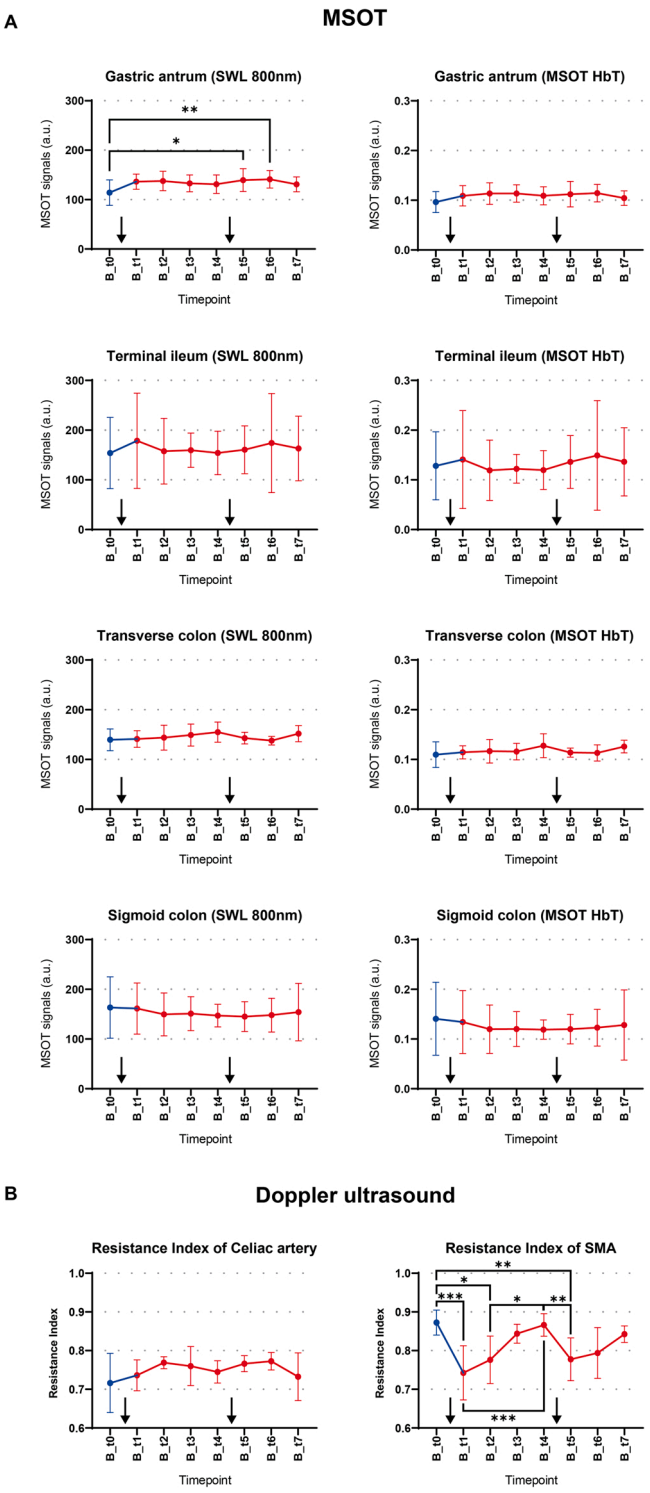

Fig. 4. Influence of food intake on MSOT and Doppler ultrasound, A Postprandial changes of MSOT signals over time. Changes of single wavelength (SWL) 800 nm and MSOT total hemoglobin (HbT) over eight imaging timepoints of day B are shown separated by anatomical region. Datapoints and whiskers represent means and standard deviation of all subjects at one imaging timepoint. Each mean consists of n = 10 datapoints (ten subjects, one datapoint derives from the mean of v1 and v2). Blue dots represent the preprandial (fasting) timepoint (t0), while postprandial timepoints are depicted in red. 30 min after the first and fifth imaging timepoint subjects ingested a standardized meal as marked with black arrows. As appropriate one-way ANOVA or mixed effects analysis for data sets with missing data and Turkey's post hoc test or Friedman test and Dunńs multiple comparisons test were used. P values < 0.05 were considered statistically significant and are depicted in the graphs with asterisks. B Postprandial changes of Doppler ultrasound (resistance index) over time Changes of resistance index over eight imaging timepoints of day B for celiac artery and superior mesenteric artery (SMA) are shown. Datapoints and whiskers represent means and standard deviation of all subjects at one imaging timepoint. Each mean consists of n = 10 measurements (ten subjects). Blue dots represent the preprandial (fasting) timepoint (t0), while postprandial timepoints are depicted in red. 30 min after the first and fifth imaging timepoint subjects ingested a standardized meal as marked with black arrows. As appropriate one-way ANOVA or mixed effects analysis for data sets with missing data and Turkey's post hoc test or Friedman test and Dunńs multiple comparisons test were used. P values < 0.05 were considered statistically significant and are depicted in the graphs with asterisks.

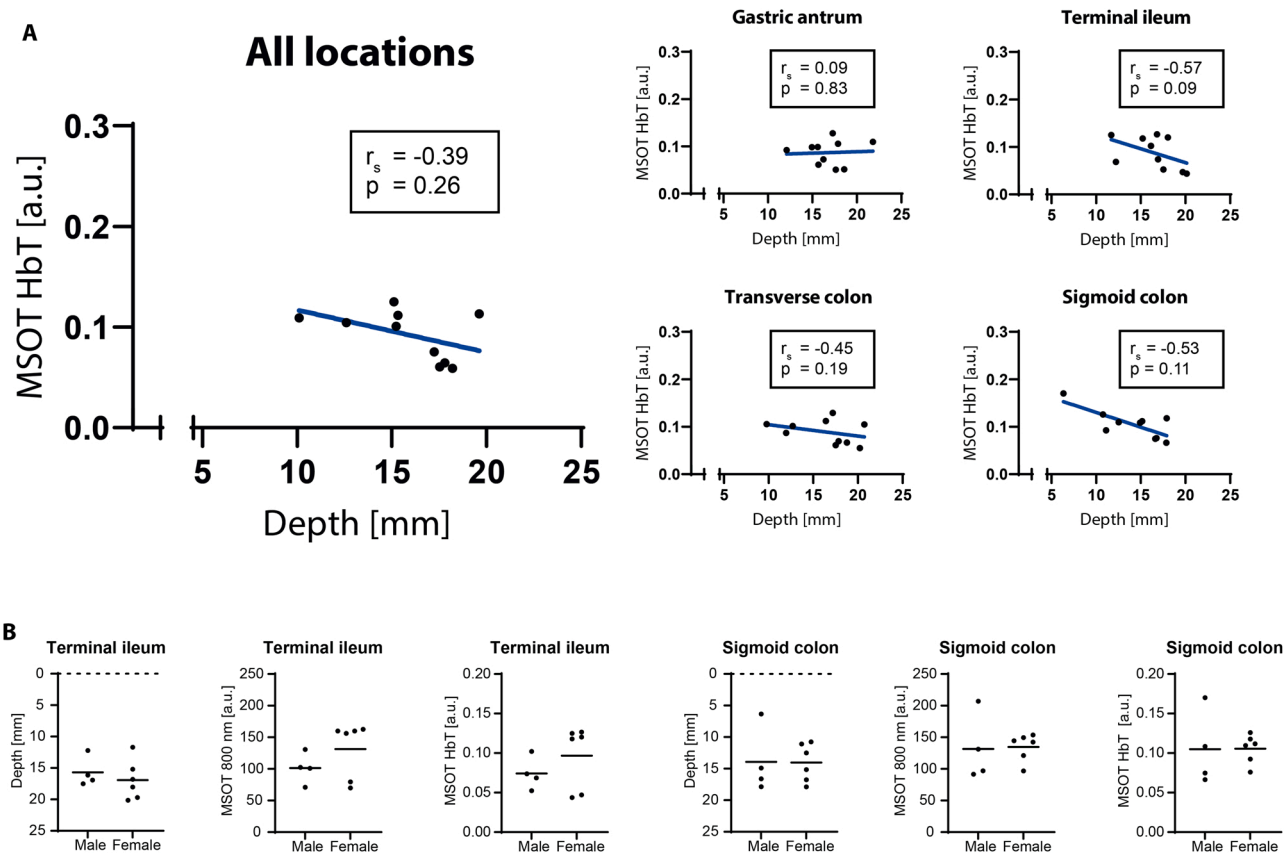

Fig. 5. Depth correlation and gender differences of MSOT signals, A Depth correlation of MSOT signals. Correlation between total hemoglobin (HbT) and region of interest (ROI) depth is shown for all anatomical locations and separated by locations. Each datapoint represents the mean from all timepoints of day A for one subject (n = 10). Parametric pearson correlation coefficient (r) and corresponding P values were computed. P values < 0.05 were considered statistically significant. Blue lines represent a simple linear regression through all datapoints. B Gender differences of MSOT signals. Differences in ROI depth, single wavelength (SWL) 800 nm and total hemoglobin (HbT) are shown for the terminal ileum and the sigmoid colon. Each datapoint represents the mean of all timepoints of day A for one subject (n = 10). Horizontal lines depict the mean of all subjects within the gender group. Comparisons between means were computed with unpaired T-test or Mann-Whitney-U test, respectively. P values < 0.05 were considered statistically significant.

value of all timepoints of day A was used. Of all locations, only the sigmoid colon showed a negative correlation between MSOT signals and ROI depth ($r = -0.76$, $P = 0.01$, Fig. 5A).

Differences of MSOT signals between sexes were assessed by comparing the mean values of male and female subjects. For each subject the mean value of all timepoints of day A was used. Herein ROI depth, and MSOT SWL 800 nm and HbT did not show any statistically significant differences between sexes in all anatomical locations (data shown for the terminal ileum and sigmoid colon in Fig. 5B.

4. Discussion

This study presents longitudinal optoacoustic imaging data of the healthy human intestine, in order to investigate physiological processes during fasting and after food intake and their influence on signal intensity and variability. While food intake increased the intestinal blood flow, MSOT signals in the bowel were consistent, fostering its potential as a diagnostic tool for the assessment of inflammation with local hyperemia in IBD [8,9].

Previous pilot studies in patients with Crohn's disease already demonstrated the ability of MSOT to grade inflammatory activity by means of optoacoustic hemoglobin signals in the bowel wall [7]. This non-invasive bedside application of MSOT might allow treatment monitoring of IBD patients with consequent reduction of invasive standard procedures, such as endoscopy. In this regard, a multicenter trial (clinicaltrials.gov ID NCT 04456400) aims to confirm the diagnostic performance of MSOT, both in patients with Crohn's disease and ulcerative colitis. However, precision of handheld MSOT for imaging the human intestine has not yet been clarified. Therefore, the present study elucidates the reliability of optoacoustic signals for various timepoints and physiological conditions in different segments of the intestine of healthy subjects.

First, when comparing two consecutive scans, within-timepoint reliability for MSOT SWLs and unmixed parameters was substantial to almost perfect for all gastrointestinal regions. However, ICCs of the terminal ileum compared to the other regions were lower. This could partially be attributed to the higher motility of the small intestine as compared to the colon [18]. Furthermore, gas overlay, stool filling as well as thin ROI areas could explain the lower ICCs compared to the values observed in muscle and soft tissue imaging [10,11].

Analysis of within-day reliability over the course of one day showed an almost perfect agreement of SWL 800 nm and HbT measurements. This is in line with the relatively small CVs in the signals across the eight imaging timepoints (14.9–33.7%).

The greater variation of spectrally unmixed HbT compared to single wavelength 800 nm might be attributed to corruption in spectral unmixing reasoned by wavelength-dependent fluence attenuation in deep tissue OAI [2]. In humans, tissue and disease-related spectral signatures are largely unknow and might interfere with supervised spectral unmixing [19].

However, spectral unmixing of endogenous chromophores is the key to resolve disease specific features in inflammatory and tumorous diseases. Furthermore, capturing of dedicated exogenous chromophores by spectral unmixing, such as indocyanine green, opens up completely new

areas of applications [20]. However, for better understanding of spectral coloring in human deep tissue, larger clinical datasets are needed, to explore advanced depth correction or to apply blind source spectral unmixing methods [19,21–23]. To facilitate the latter analysis in research collaborations, studies should be performed according to guidelines in the field [24,25] and adhere to the recommendations of the International Photoacoustic Standardization Consortium (IPASC) [26].

When comparing two separate days, between-day reproducibility measured by ICCs was rather poor. But, pertaining to CVs, the variation across the two examination days was smaller than the variation between individuals. These findings are in accordance with MRI data of the healthy intestine with similar temporal and individual variability [27], and preclinical MSOT data of murine spleens and kidneys [28]. The between-day reproducibility of MRI and MSOT signals of healthy intestine might be predominantly challenged by the difficulty of exact anatomical relocation due to missing fixed landmarks, intestinal motility, gas overlay and stool filling. Thus, within a day, it may have been somewhat more similar. Concluding, for implementation of semi-quantitative MSOT signals as outcome measures in clinical trials the increase/decrease of signals caused by the disease must be greater than individual variability. To be able to evaluate this, longitudinal studies of patients with IBD compared to healthy controls are now demanded.

Interestingly, after food intake, the only significant change in MSOT signals was an increase of the 800 nm signal in the gastric antrum. However, this finding might more likely be attributed to other confounders, such as gastric filling, as changes in the postprandial blood flow of the celiac artery, which supplies blood to the stomach, are only described during the first ten minutes after food intake [29], and were not detected by simultaneous Doppler ultrasound in this study. Moreover, no other intestinal region showed any significant changes in MSOT signals after food intake, even though increased postprandial blood flow was observed in the superior mesenteric artery, as previously described by others, too [15,30,31]. This mismatch, which was also found in studies using contrast enhanced ultrasound [32], could be explained by the fact, that the changes in postprandial blood flow in the terminal vessels inside the bowel wall are small in comparison to the main splanchnic arteries. The assumption, that food intake does not significantly alter MSOT signals in the human bowel wall, is fostered by the fact, that variation of MSOT signals was similar during fasting and after food intake.

As known from previous studies in muscles [10], imaging depth is a major confounder and limitation to light transmission [33]. Although dedicated software algorithms enable fluence correction of optoacoustic signals, a negative correlation of ROI depth and signal intensity of HbT remained in the sigmoid colon. Nevertheless, multiple variables (depth, motion, stool filling, and exact anatomical location) may also account as potential confounders. In contrast to MSOT muscle imaging [10], no gender differences were observed for intestinal imaging. This is in line with ultrasound data showing no differences in bowel wall thickness between genders [34].

This study has several limitations. First, the study investigated a relatively small number of healthy subjects and patients with IBD for group comparisons were missing. Second, training effects of the operator throughout the course of the study could have improved the positioning of the detector for optimal optoacoustic signal acquisition. In addition, the very thin bowel wall of healthy individuals led to small ROIs, which are more likely to be affected by imaging artifacts and may have led to over- or underestimation of MSOT signals. To limit this potential shortcoming, all ROIs were reviewed by two readers. Furthermore, anatomical relocation cannot be performed as precisely as during muscle imaging [10,35,36], as physiological alterations, especially gas and stool filling, require slight modifications of probe positioning. Furthermore, the inferior mesenteric artery was not assessed. Thus, the correlation between local blood supply and MSOT signals of the sigmoid colon is limited. However, the terminal ileum and transverse colon did not show relevant changes of MSOT signals, although a reduced resistance index of the superior mesenteric artery after food intake was measured in accordance with the literature [29]. Hence, subtle changes in blood circulation in the end-stream regions of the intestine might not be detected by MSOT.

In summary, reproducibility of MSOT for the evaluation of the human intestine might be considered good, especially for discriminating between healthy subjects and patients with active inflammatory bowel disease, where significantly higher MSOT hemoglobin signals are to be expected [6,7]. These findings should further support OAI technologies as component of IBD diagnostics and treatment monitoring. The implementation is suitable not only for adults, but also for children, where non-invasive biomarkers for diseases assessment are urgently needed [37]. Next, roadmaps for early feasibility studies and clinical trials in OAI should be implemented to significantly accelerate the application of OAI in clinical practice.

As an important step to this, our study determined the reproducibility and the influence of physiological alterations on MSOT signals in healthy human intestine and surfs as a framework for future MSOT studies in IBD research.

Funding

The Interdisciplinary Center for Clinical Research (IZKF) at the University Hospital of the Friedrich-Alexander-Universität (FAU) funded this project (J89 and CSP program to APR and MD-thesis scholarship to LPP). The present work was performed in fulfillment of the requirements for obtaining the degree “Dr. med.” for LPP at the Friedrich-Alexander-Universität Erlangen-Nürnberg (FAU). The project was further funded by EU H2020 research and innovation program (no. 830965 to MFN, MJW, and FK).

Author contribution

LPP, FK, and APR designed the study. FK was the principal investigator. LPP, FK, and APR performed imaging (MSOT and ultrasound). LPP, KT, DS, FK, and APR performed (statistical) data analysis. LPP and APR wrote the first draft of the manuscript. ALW and FK edited the manuscript. LPP, ALW, APB, RR, JJ, DS, KT, AS, UR, WL, AH, GS, MFN, JW, MJW, FK, and APR interpreted the data. All others approved the final version of the manuscript.

Declaration of Competing Interest

The authors declare the following financial interests/personal relationships which may be considered as potential competing interests: Markus F Neurath, Maximilian J Waldner, Ferdinand Knieling reports financial support was provided by European Union. Adrian P Regensburger reports financial support was provided by Friedrich Alexander University Erlangen Nuremberg Faculty of Medicine. Adrian P Regensburger, Ferdinand Knieling, Maximilian J Waldner has patent issued to iThera Medical GmbH, Munich, Germany. Ferdinand Knieling is a section editor of the Journal Photoacoustics, however no involved in the peer review process of this manuscript.

Data Availability

Data will be made available on request.

Acknowledgement

We thank Yi Qiu from iThera medical GmbH (Munich, Germany) for technical assistance and software support.

Conflicts of interest

MJW, FK, and APR are shared patent holders with iThera medical

GmbH (Munich, Germany) on an optoacoustic imaging system/software described in the study. FK is a section editor of the Journal Photoacoustics, however no involved in the peer review process.

Appendix A. Supporting information

Supplementary data associated with this article can be found in the online version at doi:10.1016/j.pacs.2023.100457.

References

[1] V. Ntziachristos, D. Razansky, Molecular imaging by means of multispectral optoacoustic tomography (MSOT), Chem. Rev. 110 (5) (2010) 2783–2794.
[2] S. Tzoumas, N. Deliolanis, S. Morscher, V. Ntziachristos, Unmixing molecular agents from absorbing tissue in multispectral optoacoustic tomography, IEEE Trans. Med. Imaging 33 (1) (2014) 48–60.
[3] A.P. Regensburger, E. Brown, G. Kronke, M.J. Waldner, F. Knieling, Optoacoustic imaging in inflammation, Biomedicines 9 (5) (2021).
[4] K. Tascilar, F. Fagni, A. Kleyer, S. Bayat, R. Heidemann, F. Steiger, G. Kronke, D. Bohr, A. Ramming, F. Hartmann, D. Klett, A. Federle, A.P. Regensburger, A. L. Wagner, F. Knieling, M.F. Neurath, G. Schett, M. Waldner, D. Simon, Non-invasive metabolic profiling of inflammation in joints and entheses by multispectral optoacoustic tomography, Rheumatol. (Oxf.) (2022).
[5] A.B.E. Attia, G. Balasundaram, M. Moothanchery, U.S. Dinish, R. Bi, V. Ntziachristos, M. Olivo, A review of clinical photoacoustic imaging: Current and future trends, Photoacoustics 16 (2019), 100144.
[6] M.J. Waldner, F. Knieling, C. Egger, S. Morscher, J. Claussen, M. Vetter, C. Kielisch, S. Fischer, L. Pfeifer, A. Hagel, R.S. Goertz, D. Wildner, R. Atreya, D. Strobel, M. F. Neurath, Multispectral optoacoustic tomography in crohn's disease: noninvasive imaging of disease activity, Gastroenterology 151 (2) (2016) 238–240.
[7] F. Knieling, C. Neufert, A. Hartmann, J. Claussen, A. Urich, C. Egger, M. Vetter, S. Fischer, L. Pfeifer, A. Hagel, C. Kielisch, R.S. Görtz, D. Wildner, M. Engel, J. Röther, W. Uter, J. Siebler, R. Atreya, W. Rascher, D. Strobel, M.F. Neurath, M. J. Waldner, Multispectral optoacoustic tomography for assessment of Crohn's disease activity, N. Engl. J. Med 376 (13) (2017) 1292–1294.
[8] L. Hultén, J. Lindhagen, O. Lundgren, S. Fasth, C. Ahrén, Regional intestinal blood flow in ulcerative colitis and Crohn's disease, Gastroenterology 72 (3) (1977) 388–396.
[9] T.J. Williams, M.J. Peck, Role of prostaglandin-mediated vasodilatation in inflammation, Nature 270 (5637) (1977) 530–532.
[10] A.L. Wagner, V. Danko, A. Federle, D. Klett, D. Simon, R. Heiss, J. Jüngert, M. Uder, G. Schett, M.F. Neurath, J. Woelfle, M.J. Waldner, R. Trollmann, A. P. Regensburger, F. Knieling, Precision of handheld multispectral optoacoustic tomography for muscle imaging, Photoacoustics 21 (2021), 100220.
[11] A. Helfen, M. Masthoff, J. Claussen, M. Gerwing, W. Heindel, V. Ntziachristos, M. Eisenblatter, M. Kohler, M. Wildgruber, Multispectral optoacoustic tomography: intra- and interobserver variability using a clinical hybrid approach, J. Clin. Med 8 (1) (2019).
[12] P.J. Matheson, M.A. Wilson, R.N. Garrison, Regulation of intestinal blood flow, J. Surg. Res 93 (1) (2000) 182–196.
[13] P.R. Kvietys, Integrated systems physiology: from molecule to function, the gastrointestinal, Circulation (2010).
[14] C.C. Chou, C.P. Hsieh, Y.M. Yu, P. Kvietys, L.C. Yu, R. Pittman, J.M. Dabney, Localization of mesenteric hyperemia during digestion in dogs, Am. J. Physiol. 230 (3) (1976) 583–589.
[15] K. Jäger, A. Bollinger, C. Valli, R. Ammann, Measurement of mesenteric blood flow by duplex scanning, J. Vasc. Surg. 3 (3) (1986) 462–469.
[16] R.S. Goertz, C. Egger, M.F. Neurath, D. Strobel, Impact of food intake, ultrasound transducer, breathing maneuvers and body position on acoustic radiation force impulse (ARFI) elastometry of the liver, Ultraschall Med 33 (4) (2012) 380–385.
[17] J.R. Landis, G.G. Koch, The measurement of observer agreement for categorical data, Biometrics 33 (1) (1977) 159–174.
[18] M. Rao, An increasingly complex view of intestinal motility, Nat. Rev. Gastroenterol. Hepatol. 17 (2) (2020) 72–73.
[19] V. Grasso, H.W. Hassan, P. Mirtaheri, R. Willumeit-Römer, J. Jose, Recent advances in photoacoustic blind source spectral unmixing approaches and the enhanced detection of endogenous tissue chromophores, Front. Signal Process. 2 (2022).
[20] I. Stoffels, S. Morscher, I. Helfrich, U. Hillen, J. Leyh, N.C. Burton, T.C. Sardella, J. Claussen, T.D. Poeppel, H.S. Bachmann, A. Roesch, K. Griewank, D. Schadendorf, M. Gunzer, J. Klode, Metastatic status of sentinel lymph nodes in melanoma determined noninvasively with multispectral optoacoustic imaging, Sci. Transl. Med 7 (317) (2015) 317ra199.
[21] J. Vonk, J. Kukacka, P.J. Steinkamp, J.G. de Wit, F.J. Voskuil, W.T. R. Hooghiemstra, M. Bader, D. Justel, V. Ntziachristos, G.M. van Dam, M.J. H. Witjes, Multispectral optoacoustic tomography for in vivo detection of lymph node metastases in oral cancer patients using an EGFR-targeted contrast agent and intrinsic tissue contrast: A proof-of-concept study, Photoacoustics 26 (2022), 100362.
[22] H. Zuo, M. Cui, X. Wang, C. Ma, Spectral crosstalk in photoacoustic computed tomography, Photoacoustics 26 (2022), 100356.
[23] J. Grohl, T. Kirchner, T.J. Adler, L. Hacker, N. Holzwarth, A. Hernandez-Aguilera, M.A. Herrera, E. Santos, S.E. Bohndiek, L. Maier-Hein, Learned spectral decoloring enables photoacoustic oximetry, Sci. Rep. 11 (1) (2021) 6565.
[24] W. Heeman, J. Vonk, V. Ntziachristos, B.W. Pogue, R. Dierckx, S. Kruijff, G.M. van Dam, A guideline for clinicians performing clinical studies with fluorescence imaging, J. Nucl. Med 63 (5) (2022) 640–645.
[25] S. Bohndiek, Addressing photoacoustics standards, Nat. Photonics 13 (5) (2019), 298-298.
[26] J. Grohl, L. Hacker, B.T. Cox, K.K. Dreher, S. Morscher, A. Rakotondrainibe, F. Varray, L.C.M. Yip, W.C. Vogt, S.E. Bohndiek, C, Members of the International Photoacoustic Standardisation, The IPASC data format: a consensus data format for photoacoustic imaging, Photoacoustics 26 (2022), 100339.
[27] A.S. Alyami, H.G. Williams, K. Argyriou, D. Gunn, V. Wilkinson-Smith, J.R. White, J. Alyami, P.A. Gowland, G.W. Moran, C.L. Hoad, Test-retest assessment of non-contrast MRI sequences to characterise and quantify the small bowel wall in healthy participants, Magma 34 (6) (2021) 791–804.
[28] J. Joseph, M.R. Tomaszewski, I. Quiros-Gonzalez, J. Weber, J. Brunker, S. E. Bohndiek, Evaluation of precision in optoacoustic tomography for preclinical imaging in living subjects, J. Nucl. Med 58 (5) (2017) 807–814.
[29] N. Someya, M.Y. Endo, Y. Fukuba, N. Hayashi, Blood flow responses in celiac and superior mesenteric arteries in the initial phase of digestion, Am. J. Physiol. -Regul., Integr. Comp. Physiol. 294 (6) (2008) R1790–R1796.
[30] M.J. Perko, Duplex ultrasound for assessment of superior mesenteric artery blood flow, Eur. J. Vasc. Endovasc. Surg. 21 (2) (2001) 106–117.
[31] P. Taourel, P. Perney, M. Dauzat, B. Gallix, J. Pradel, F. Blanc, L. Pourcelot, J. M. Bruel, Doppler study of fasting and postprandial resistance indices in the superior mesenteric artery in healthy subjects and patients with cirrhosis, J. Clin. Ultrasound 26 (3) (1998) 131–136.
[32] G. Maconi, A.K. Asthana, E. Bolzacchini, A. Dell'Era, F. Furfaro, C. Bezzio, V. Salvatore, J.A. Maier, Splanchnic hemodynamics and intestinal vascularity in Crohn's disease: an In Vivo evaluation using doppler and contrast-enhanced ultrasound and biochemical parameters, Ultrasound Med Biol. 42 (1) (2016) 150–158.
[33] A. Oraevsky, S. Jacques, R. Esenaliev, F. Tittel, Laser-based optoacoustic imaging in biological tissues, SPIE, OE/LASE '94, 1994, Los Angeles, CA, United States, 1994.
[34] K. Nylund, T. Hausken, S. Ødegaard, G.E. Eide, O.H. Gilja, Gastrointestinal wall thickness measured with transabdominal ultrasonography and its relationship to demographic factors in healthy subjects, Ultraschall Med 33 (7) (2012) E225–e232.
[35] A.P. Regensburger, L.M. Fonteyne, J. Jungert, A.L. Wagner, T. Gerhalter, A. M. Nagel, R. Heiss, F. Flenkenthaler, M. Qurashi, M.F. Neurath, N. Klymiuk, E. Kemter, T. Frohlich, M. Uder, J. Woelfle, W. Rascher, R. Trollmann, E. Wolf, M. J. Waldner, F. Knieling, Detection of collagens by multispectral optoacoustic tomography as an imaging biomarker for Duchenne muscular dystrophy, Nat. Med 25 (12) (2019) 1905–1915.
[36] A.P. Regensburger, A.L. Wagner, V. Danko, J. Jungert, A. Federle, D. Klett, S. Schuessler, A. Buehler, M.F. Neurath, A. Roos, H. Lochmuller, J. Woelfle, R. Trollmann, M.J. Waldner, F. Knieling, Multispectral optoacoustic tomography for non-invasive disease phenotyping in pediatric spinal muscular atrophy patients, Photoacoustics 25 (2022), 100315.
[37] A.P. Regensburger, A.L. Wagner, J. Claussen, M.J. Waldner, F. Knieling, Shedding light on pediatric diseases: multispectral optoacoustic tomography at the doorway to clinical applications, Mol. Cell Pedia 7 (1) (2020) 3.

Lars-Philip Paulus is a medical student at the Friedrich-Alexander Universität Erlangen-Nürnberg. He is working on his MD thesis in the Pediatric and Experimental Imaging Laboratory of Dr. Ferdinand Knieling since 2020. He is dedicated to optoacoustic imaging with special regard to (pediatric) inflammatory bowel diseases.

Dr. Adrian P. Regensburger is a clinician scientist at the Department of Pediatric and Adolescent Medicine at the University Hospital Erlangen and the Pediatric and Experimental Imaging Laboratory of Dr. Ferdinand Knieling. He is consultant of the pediatric Department of Gastroenterology and Hepatology with special interest to inflammatory bowel diseases and the application of novel imaging modalities.